Two-Dimensional Microscale Engineering of Protein-Based Nanoparticles for Cell Guidance

Witold I. Tatkiewicz,[†,‡] Joaquin Seras-Franzoso,[‡,§,⊥] Elena García-Fruitós,[‡,§] Esther Vazquez,[‡,§,⊥] Nora Ventosa,[†,‡] Karl Peebo,[§,∥] Imma Ratera,[†,‡,*] Antonio Villaverde,[‡,§,⊥] and Jaume Veciana[†,‡,*]

[†]Department of Molecular Nanoscience and Organic Materials, Institut de Ciencia de Materials de Barcelona (CSIC), Bellaterra, 08193 Barcelona, Spain, [‡]CIBER de Bioingeniería, Biomateriales y Nanomedicina (CIBER-BBN), Bellaterra, 08193 Barcelona, Spain, [§]Institut de Biotecnologia i de Biomedicina (IBB), Universitat Autònoma de Barcelona, Bellaterra, 08193 Barcelona, Spain, [⊥]Department of Genetics and Microbiology, Universitat Autònoma de Barcelona, Bellaterra, 08193 Barcelona, Spain, and [∥]Competence Center of Food and Fermentation Technologies, Akadeemia tee 15a, 12618 Tallinn, Estonia

ABSTRACT Cell responses, such as positioning, morphological changes, proliferation, and apoptosis, are the result of complex chemical, topographical, and biological stimuli. Here we show the macroscopic responses of cells when nanoscale profiles made with inclusion bodies (IBs) are used for the 2D engineering of biological interfaces at the microscale. A deep statistical data treatment of fibroblasts cultivated on supports patterned with green fluorescent protein and human basic fibroblast growth factor-derived IBs demonstrates that these cells preferentially adhere to the IB areas and align and elongate according to specific patterns. These findings prove the potential of surface patterning with functional IBs as protein-based nanomaterials for tissue engineering.

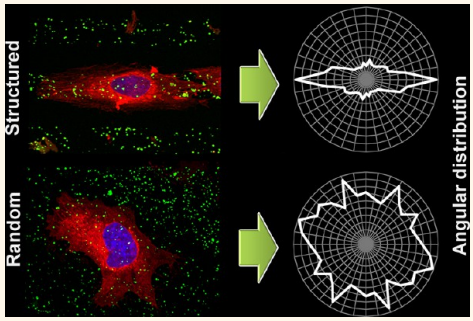

KEYWORDS: inclusion bodies · protein nanoparticles · cell guidance · 2D engineering · fibroblasts · microcontact printing · tissue engineering

Cell responses such as positioning, migration, morphological changes, proliferation, and apoptosis are the result of a complex network of stimuli transmitted by the extracellular matrix (ECM). Among them, mechanical (topography, internal constrains), chemical (presence and concentration of different effector molecules), and biological (influence of other cells, growth factors, and signal transducers) factors predestine the cellular fate. Mimicking the physiological conditions and environmental topography of natural systems at the cell scale is one of the basic aims of tissue engineering that is hoped to open new opportunities in regenerative medicine.

Several techniques are being applied to investigate the influence of these stimuli on cells in order to gain know-how and control over cell proliferation and eventually tissue generation. Among them, microcontact printing (μCP) is recognized as a cost-effective, fast, and versatile technique to control surface chemistry driving properties at the microscale.[1] The range of materials that can be used to cover surfaces using this method is very broad:[2,3] from self-assembled monolayers (SAMs),[4] proteins,[5,6] and nucleic acids[7] to more complex architectures[8] giving rise to functional surfaces,[9] which are obtained by multistep protocols. Although in most cases the "ink" used in this printing procedure consists of a solution of the molecules of interest, such soft-lithographic method can also be extended to pattern colloidal particles[10] or even bacteria.[11] Other approaches use hard-lithographic techniques to study cell responses to topography.[12,13] By these techniques, cell orientation and morphological changes in response to the modification of the surface topography are being explored,[14] and the relationship between the substrate topography and the formation of filopodia, lamellipodia, and focal adhesion points is being evaluated.[15,16] Cells have also been shown to follow the orientation of carbon nanotubes[17] and to react positively to subtle differences induced by the presence of nanobeads on the substrate.[18]

Recently, approaches that focus on two or more of the previously described techniques have been reported. Thus, Charest *et al.*

* Address correspondence to vecianaj@icmab.es, iratera@icmab.es.

Received for review October 15, 2012 and accepted May 24, 2013.

Published online May 24, 2013
10.1021/nn400907f

applied both the hot embossing technique and the μCP to obtain substrates with grooves covered with perpendicular stripes of proteins.[19] Feinberg *et al.* presented a similar architecture but with parallel patterns, also using a multistep protocol.[20] An interesting study was presented by Recknor *et al.* where astrocytes cocultured with adult rat hippocampal progenitor cells over chemically modified micropatterned polystyrene substrates were shown to preferentially acquire neuronal morphology depending on the microstructuration of the substrate.[21] All of these examples are indications that substrate topography, in synergy with chemical modification and biological guidance cues, facilitates cell guidance and differentiation.

Regarding the quantification of the complex cell–substrate interactions for the analysis of all previously mentioned techniques, to the best of our knowledge, there are no available methods that deliver statistically relevant results, as most of them are limited by the use of a few cell images or by eye counting. One pioneering study in this context was an innovative cell counting assay using quantum dots to compare cell adhesion data by means of an automated image recognition software developed by Parak *et al.*[22]

In contribution to this area of research, our group has used bacterial inclusion bodies (IBs) formed by the *Aequorea victoria* green fluorescence protein (GFP) as biologically inert nanobiomaterials to explore possible synergies between some of the aforementioned approaches. IBs are highly pure protein nanoparticles produced by recombinant bacteria, ranging from around 50 nm to a few hundred nanometers in diameter. Produced through biological synthesis,[23] IBs are fully biocompatible, preserve the functionality of the embedded protein,[24] show tunable sizes and geometries, and have slightly negatively charged surfaces.[25] In addition, their production and downstream processes are fully scalable and methodologically simple.[26] Recently, it has been shown that when IBs are used as particulate materials to engineer the nanoscale topography, cell culture is assisted, proving a positive impact on colonization and proliferation.[27,28] Besides, as IBs are highly bioadhesive materials, a mammalian cell expansion on IB-decorated surfaces has been proven to be synergistically supported by both favored adhesion and mechanical stimulation of cell division, as determined by the enhanced phosphorylation of the signal-regulated protein kinase and by the dramatic emission of filopodia in the presence of IBs.[29] Moreover, the intrinsic proteinaceous nature of IBs might avoid any possible screening or coverage of the nanoparticles with protein corona or largely reduce its functional impact upon their entrance to the biological medium.[30] The absence of protein corona has been verified by measuring the size of IBs with and without serum, not finding any apparent change.

On the other hand, it has been found that the chemical, morphological, and mechanical properties of IBs can be controlled by the proper choice of the genetic background of the producing bacteria.[24] The fact that all of these parameters influence the cell growth proves that the actual range of IB mechanical properties is sensed and discriminated by biological systems, opening exciting possibilities for the fine tailoring of protein nanoparticle features that are relevant in tissue engineering.[28] Although it is known that IBs are promising nanomaterials for tissue engineering because they combine biofunctionality and the nanoscopic topography, nothing is known about the influence of surface modification with these nanoparticles on the global spatial organization of cells. In this context, here we have explored the macroscopic guidance of cells when IB nanoscale profiling is used for the 2D engineering of biological interfaces at the microscale.

To perform such studies, we have developed a novel method that allows a deep statistical image analysis of fibroblasts cultured on supports decorated with fluorescent IBs. Such a method is based on the automatized modelization of the shape of nuclei and membrane of cells by ellipses, which allows the positions of cells on a given surface to be known and their morphology by means of the ratio between their long- and short-axis as well as the orientation of the cell to be estimated, as determined by the angle of the long-axis of the ellipse with respect a reference direction of the surface. To apply this method, we used several patterns of IBs with various shapes and sizes to study the behavior of cells. Finally, as a proof of concept, we have also applied the developed statistical method to surfaces patterned with biofunctional IBs formed by the human basic fibroblast growth factor (FGF) to expand the usefulness of these novel protein-based and highly versatile nanomaterials in the field of tissue engineering. This method allows one to guide the cell growth on substrates as a function of the morphology of a template by using novel protein-based nanoparticles, that is, for the production of aligned cell rows when grown on the grating of an appropriate interseparation, which is of fundamental interest in the field of regenerative medicine of tissues that need to be morphologically organized.

RESULTS AND DISCUSSION

To accomplish all of these objectives, we have selectively decorated substrates with GFP-derived IBs using a modification of the μCP technique, in order to ensure a reliable and enhanced transferring of the proteinaceous nanoparticles to premodified silicon substrates with amino-terminated SAMs. We have shown that a modification of the stamp surface, by dipping a polydimethylsiloxane (PDMS) stamp in a solution of sodium dodecyl sulfate (SDS) surfactant, before its immersion into the IB suspension, enhances the detachment of IBs from the stamp, due to the formation of a release layer which enhances its transfer onto such substrates.[31]

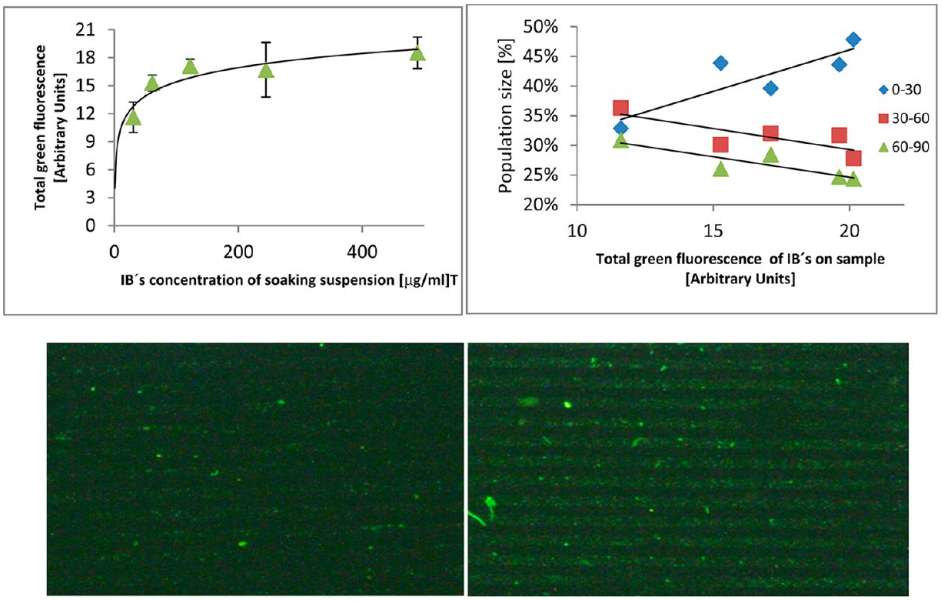

Figure 1. Optimization of the IBs coverage. Top (Left) Total green fluorescence intensity emitted by substrates patterned with 20 μm stripes using PDMS stamps inked with suspensions of GFP-derived IBs at different concentrations (489, 244, 122, 61, and 30 $\mu g \cdot mL^{-1}$) in PBS solutions. Note that acquired images were taken under the same exposure conditions. Logarithmic fitted curve is shown as guidance. (Right) Comparison between the resulting populations of well, medium, and wrong oriented cell membranes, appearing with 0−30° (blue), 30−60° (red), and 60−90° (green) angles (see text) obtained for 20 μm stripes patterned substrates with increasing IB densities. Straight lines are shown as guidance. Bottom: Images of patterned substrates with 20 μm stripes using concentrations of GFP-derived IBs of 122 (left) and 244 $\mu g \cdot mL^{-1}$ (right).

In order to determine the optimal density of IBs for cell proliferation and guidance experiments, we have cultured cells over supports with 20 μm wide stripes in which we varied the density of IBs covering the surfaces. For that, we used the modified μCP technique with suspensions of IBs at different concentrations in phosphate buffered saline (PBS) solutions as ink. We succeeded in obtaining, in a reproducible manner, supports with the same geometric pattern (20 μm stripes) but with different density of IB particles (see Figure 1 and Supporting Information Figure S1). The different densities of IBs achieved were quantified by determining the average intensity of the green fluorescence emitted by the GFP-derived IBs on the patterned surfaces. Figure 1 shows the dependence of total green fluorescence, emitted by the IBs on the patterned substrate, on the particle concentration used in the ink. From this graph, we can conclude that the amount of IBs that can be transferred by the modified μCP technique is limited by saturation, and that at concentrations higher than 200 $\mu g \cdot mL^{-1}$ an augment of the IBs' concentration in the ink does not increase the amount of deposited material on the surface significantly.

To perform a statistical analysis on the influence of IBs' density on cell (nuclei and membrane) orientation, 1BR3.G human skin fibroblasts were cultured on patterned surfaces with different IB densities (Figure S2). Figure 1 (top, right) shows the dependence on surface density of IBs of the populations of well, medium, and wrong oriented cell membranes, as defined by cells showing angles between the long-axis of the ellipse and the direction of stripes of 0−30, 30−60, and 60−90°, respectively. From these plots, it was observed that cells are better oriented when cultured on patterns with high IB densities. In addition, from these preliminary experiments, we also conclude that the optimal working density of IBs on surfaces is the one obtained by soaking the stamps in the suspension of IBs with a concentration of 240 $\mu g \cdot mL^{-1}$. In fact, surfaces obtained from higher concentrations do not lead to much higher densities of IBs on the surfaces due to saturation effects, and on the other hand, surfaces with lower densities of IBs show poorer cell guidance properties.

Once we determined the optimal IB density, we investigated the influence on cell guidance in four different pattern geometries on premodified silicon substrates with amino-terminated SAMs using in all cases the optimal IB concentration. We used stripes of 5, 20, and 50 μm width (spaced the same distances) and dots of 20 μm diameter (spaced correspondingly). We also added two controls to our array of substrates, namely, a surface with randomly distributed IBs, obtained with the optimal IB density, and IB-free surfaces, denoted as "Random" and "Blank", respectively. On these microstructured substrates, 1BR3.G human skin fibroblasts were cultured for 24, 48, and 72 h, and both nuclei and membrane were stained for bright-field (Figures 2, S3, S5, and S6), fluorescence, and confocal microscopies (Figure 3). The obtained images of the cells were modeled with ellipses and used to perform a

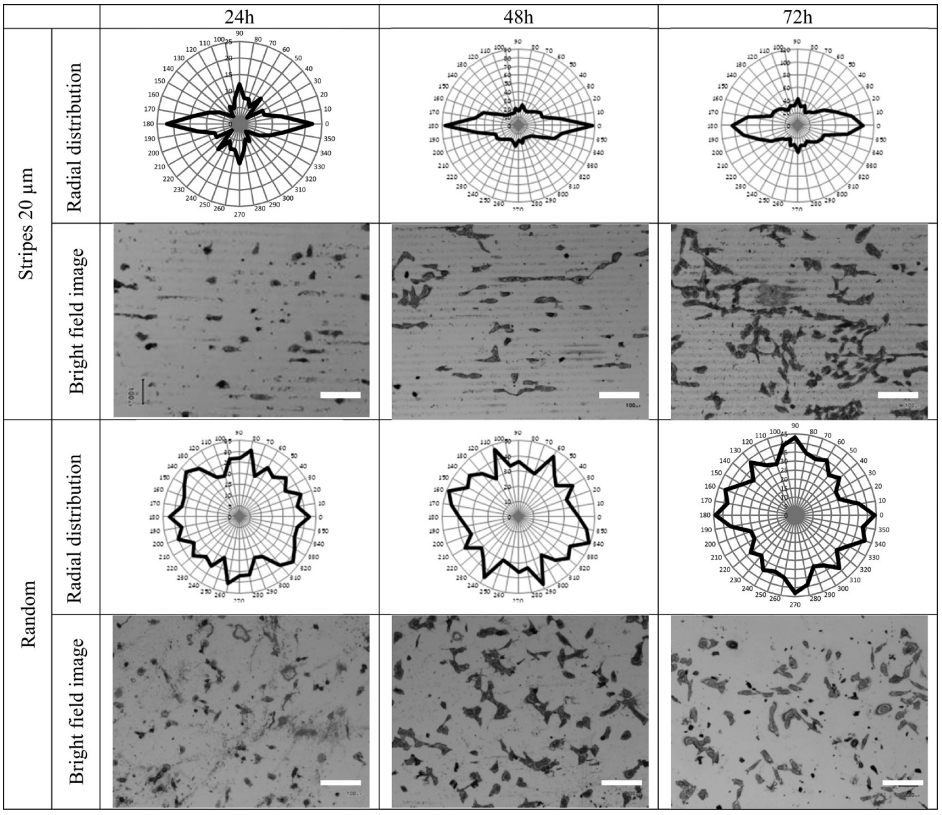

Figure 2. Impact of IB patterning and culture time on the orientation of 1BR3.G fibroblast cells. Radial distribution plots of cell membrane orientation *versus* the frequency of appearance of cells cultivated on surfaces with patterned stripes during 24, 48 and 72 h. Such plots are juxtaposed with representative bright-field optical microscopy images. Data for stripes of 20 μm and random pattern are shown here, while those corresponding to other stripes, dots, and a blank surface are given in the Supporting Information. The spindle-like distribution for the pattern with stripes is an indication of a strong guidance of the cell orientation. Bar length indicates 200 μm.

statistical analysis to investigate the influence of the different IB microscale structuration on cell orientation, positioning, and morphology. The absence of a protein corona or effects on guidance has also been verified by repeating the experiments without serum.

Representative bright-field optical microscopy images of 1BR3.G human skin fibroblasts cultured for 24, 48, and 72 h on the different patterned IB geometries are shown in Figures 2 and S3. A well-pronounced structuration of IBs is visible for all the patterns, proving that the modification of the μCP protocol was successful. Cell proliferation and morphological changes are observed in all cases, evidencing the biocompatibility of the nanopatterned material. Unlike many other related researchers in the field, we have not changed the local wettability of the supports, letting cells adhere freely all over the sample surface, a fact that enabled us to determine the specific influence of IB patterns on cell guidance. As GFP-derived IB patterns emitted sufficient green fluorescence, we therefore investigated in detail the statistical correlation between the occurrence of IBs and cells. This was accomplished for the green, red, and blue fluorescent profiles obtained from the analysis of the images (Figure 3). Profiles of the green fluorescence originated from the IBs were well-depicted for all patterned supports, demonstrating the effectiveness of the patterning by the μCP technique. To gain insights into cell positioning, we determined for each color channel the average intensity of each pixel line along the pattern (see Figure 3) and represented these data as fluorescent intensity *versus* distance profiles of the green, red, and blue fluorescence originating, respectively, from the IBs, cell membrane, and cell nuclei. A good correlation between the occurrence of IBs and the presence of cells (membrane and/or nuclei) can be seen for patterns with 20 and 50 μm stripes and to a lesser extent for 20 μm dots. In contrast for the 5 μm stripes, peaks of blue (nuclei) and red (membrane) fluorescence were much wider than the green peaks of the IB pattern, due to the wider size of the cell in comparison with the patterned IB stripes. In the random control sample, it can be observed that, even without any pattern, a higher concentration of IBs leads to an increased concentration of cells.

In order to make a comparison between the different patterns, we calculated for every channel of emitted fluorescence (red, green, and blue), separately, the ratio between the fluorescence coming from inside the patterned areas and the fluorescence from outside such areas. This ratio, named *advantage ratio*, enables a

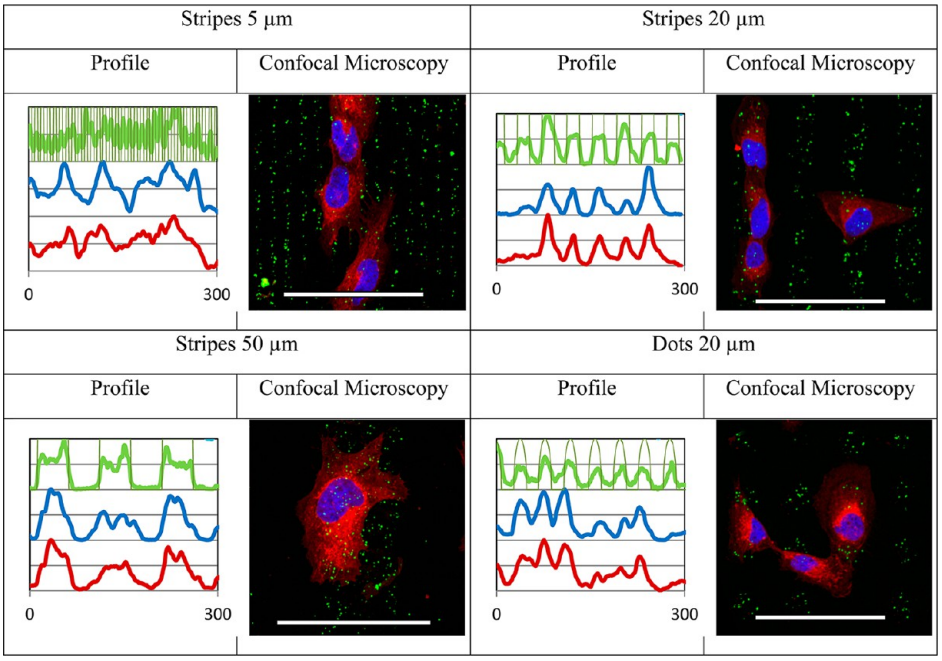

Figure 3. Impact of patterned geometry of IBs on the position of 1BR3.G fibroblasts after 48 h of culture. Examples of local profiles of the averaged fluorescence produced by the GFP-derived IBs (green), membrane (red; stained with CellMask), and nuclei (blue; stained with Hoechst) of cells are juxtaposed with a representative confocal microscopy image. Red, cellular membrane; blue, cellular nuclei; green, IB (GFP); and light green, the "ideal" IB profile. Local profiles are normalized so that the maximal and minimal values are 1 and 0, respectively. Bar length indicates 100 μm.

quantitative estimate of the amounts of IBs deposited on the patterned surfaces as well as the amount of cells growing on the IB-covered regions in comparison with those on the IB-free ones. The advantage ratio coming from the green fluorescence shows that there is at least two times more green fluorescence inside than outside the ideal pattern region (Figure S4). Moreover, the higher values of advantage ratios obtained for the wider patterns suggest that such patterned areas are much better defined than the smaller ones, enabling one to perform a pattern validation. This result can be explained by the fact that wider patterns facilitate the adhesion of IBs to the stamp, improving the transfer to the prefunctionalized silicon supports. The values of advantage ratio obtained from the red channel signal for membranes of cells cultured at different times on distinct patterned surfaces are presented in Figure 4A, where it is clearly shown that for the 5 μm stripes, the ratio of red fluorescence between the inside and outside of the patterned areas is close to 1. This is in good agreement with the fact that cells are much bigger than the size of such stripes and consequently they adhere to more than one stripe at the same time, covering the areas between the stripes of IBs (see Figure 3). The higher values of the advantage ratio observed for the 20 μm striped patterns and even much higher for the 50 μm patterns suggest that the areas with IBs are preferred by the cells, especially after the first 24 h of culture. Another interesting observation is that the advantage ratio values decrease with time as an effect of the limited available space for cells on the patterned areas and proliferation of cells also occurs over undecorated areas. Thus, after 72 h, the advantage ratio is close to 1 for most of the cases, indicating that all regions are almost equally covered with cells (see also Figure S3).

These data are in agreement with previous studies in which nanotopographies generated by colloidal lithographic methods significantly favored the attachment of fibroblasts at early culture times.[32] Interestingly, not only the size of nanocues but also their stiffness, chemical composition, and distribution have been shown to affect cell responses.[33,34] Thus, irregular distribution of the nanomechanical stimuli provided by IBs would enhance cell adhesion upon seeding, prompting higher cell coverage of the IB-patterned areas, a result that is more evident at 24 h and that progressively fades out at longer culture times.

Subsequent to the positioning analysis of cultured fibroblasts, we also investigated their orientation as well as the change of morphology induced by the different IB patterns. In Figure 2, examples of distribution of orientation angles of the cell membrane for the 20 μm stripes and the random pattern are presented at different proliferation times. The data of the other patterns are available in Figure S5. For all striped patterns, it can be clearly observed that the angular distributions present an unambiguous tendency to align along the stripes (horizontal direction). Even though, it can be observed that, after the first 24 h, there is a broader distribution of membrane orientations on the 50 μm stripes, which is indicative that cells

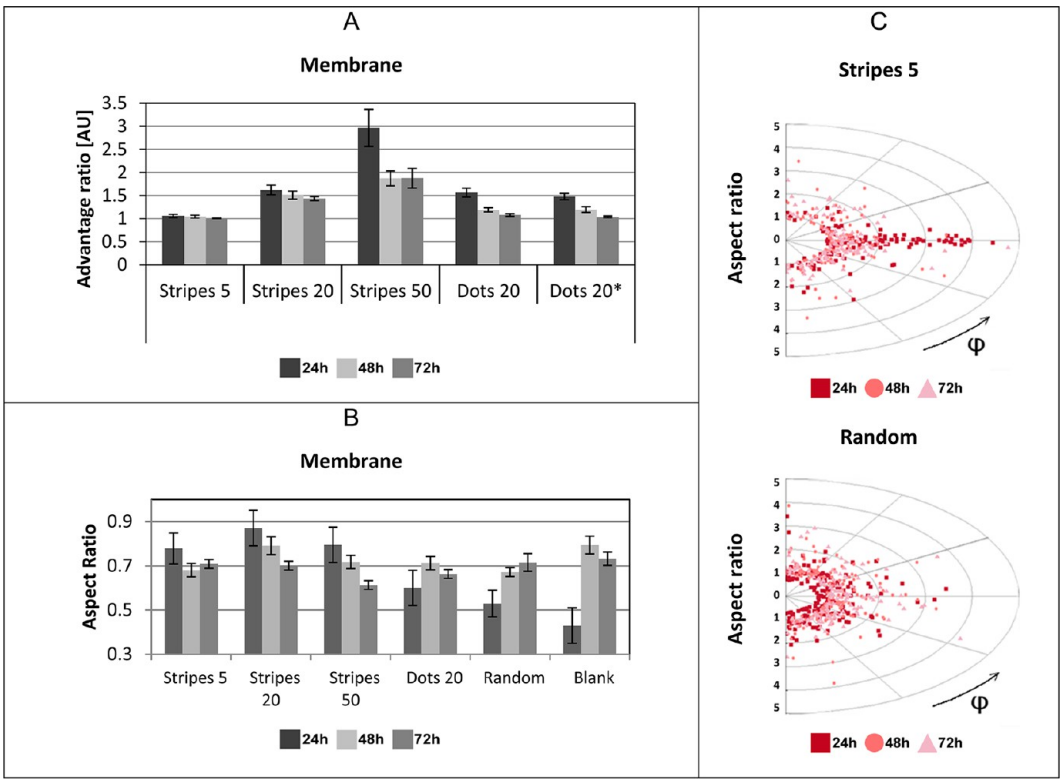

Figure 4. Influence of IB-modified substrates on the cell positioning, orientation, and morphology. (A) Advantage ratios of fluorescence signals inside and outside the IB-patterned regions coming from the red fluorescence of stained membranes. Dots were analyzed in both horizontal and vertical (marked with an asterisk) directions. An advantage ratio of 1 is an indication that cells are localized equally over patterned and unpatterned regions. The higher the values, the bigger the concentration of cell membranes over the patterned regions. It has to be taken into account the fact that IBs patterned in stripes or dots cover 50 and 19.6% of the whole surface, respectively. (B) Average aspect ratios (see main text) of cells cultivated on patterned surfaces where the evolution of cell elongation with time can be traced for each pattern. (C) Membrane aspect ratio *versus* orientation angles of cells cultivated on 5 μm striped surfaces and on a surface with randomly distributed IBs and its evolution with time. Each dot represents the cell's elongation value for each pattern, and the angle from the horizontal line corresponds to the orientation of cells. Colors represent different times of cultivation.

still have some degree of freedom to orient themselves because of the larger preferred IB pattern area in comparison with the cell size (see also Figure 3). On the contrary, the 20 μm stripes almost match the cell size and, therefore, a narrower distribution of orientations of cells is observed in this case at all proliferation times (Figure 2). Surprisingly, despite the fact that on the 5 μm striped pattern the cells grow over more than one stripe (Figure 3), the distribution of orientations in this case is kept very narrow and well-pronounced (see Figure S5) at early times. However, this tendency changes with time, and a broadening of the orientation distribution is progressively observed. The distribution for the 5 μm stripes broadens faster than for the 20 μm and for the 50 μm ones, in which it remains constant. It is worth mentioning that, after 72 h, cells growing over the 20 μm patterns still maintain their orientation. Analogous analyses for the nuclei of cells cultured on all patterned surfaces can be seen in Figure S6, leading to similar conclusions.

Regarding the cells growing on dotted patterns, it is observed that at early experimental times they do not show any preferential direction. However, after 48 h of culture, directions close to 0 and 90° became more pronounced (Figures S3, S5, and S6). We attribute this bimodal distribution to the fact that cells elongate to reach neighboring dots, spending less effort directing along dot rows and columns, as similarly reported by Charest *et al.*[35] A coarse-grained analysis of these data highlights this event even more (see Figure S7). Similar analysis performed for the nuclei shows that the orientation of this cellular compartment follows the same orientation as the whole cell (Figure S7).

Apart from the cell positioning and its orientation, IB-patterned substrates also govern the morphology of cells. In Figure 4B, the average elongation of cell membranes, named aspect ratio, is presented, which is defined by the ratio between the cell's largest and smallest sizes minus one, attained by cells cultured on the different patterned substrates. Fibroblasts growing on striped supports for a short period of time presented a high aspect ratio that decreases with time. On the contrary, cells growing on supports without patterns showed an initially round membrane morphology (low values of aspect ratio) that progressively became more elongated. Moreover, after 72 h, cells present similar

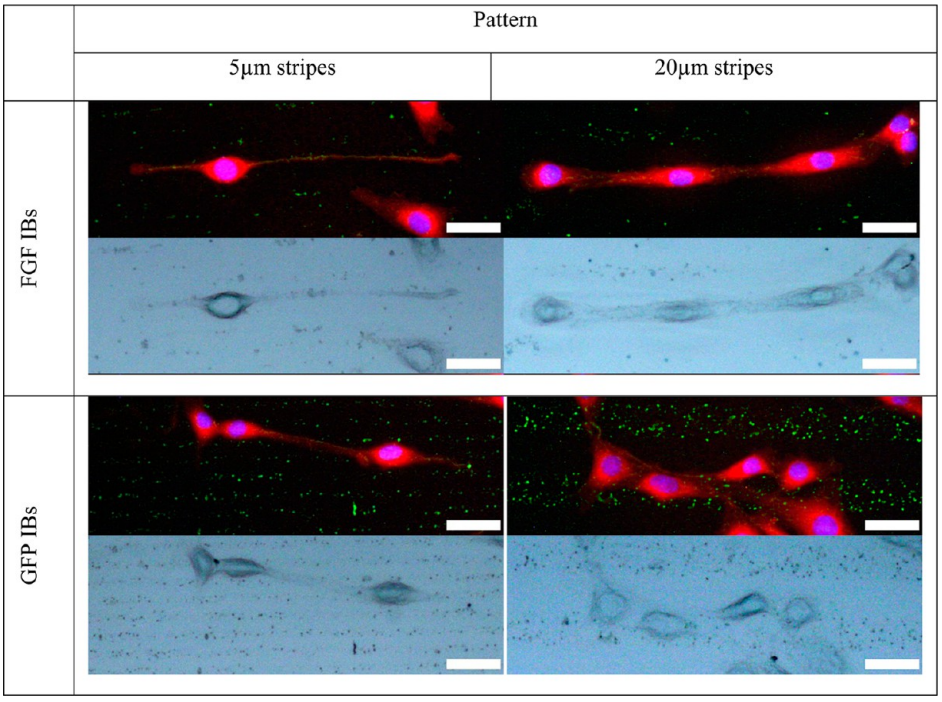

Figure 5. Bright-field and merged fluorescence images of NIH/3T3 cells cultured over FGF- and GFP-derived IBs for 24 h using inks with concentrations of 9 and 240 $\mu g \cdot mL^{-1}$, respectively, for the μCP. Red, membrane; blue, nuclei; green, IBs. Scale bar indicates 30 μm.

elongations in all the supports. Interestingly, cells growing over randomly distributed IBs showed a more elongated initial morphology than those growing on bare supports without IBs. This fact is an indication that IBs are acting as efficient focal adhesion points, as evidenced in Figure S9 by the clear formation of filopodia and lamellipodia in contact with the IBs on the surface. This result confirms our previous observations that the cellular adhesion to IBs is stronger than that attained on standard supports.[29]

To analyze the effect of the patterns on the cell elongation, we also analyzed the correlation between the aspect ratio and the orientation angles of cells as well as its evolution with time (Figures 4C and S10). From the resulting plots, it can be seen that in all cases cells were more elongated in the direction of the patterns, which is an indication of pattern-mediated cell morphology guidance. Also, in the case of the dotted pattern, a bimodal distribution of morphology emerged as previously described (Figure S10). Therefore, the combination of nanoscale features of IBs that provide a highly adhesive environment with the morphological guidance determined by the microscale patterns clearly affects cell behavior. Control of cell responses at nano/microscales has proved to be a powerful tool in order to trigger mechano-transductive events as well as direct tensegrity processes able to lead a gene expression shift with implications in such diverse cell responses such as adhesion, proliferation, spreading, differentiation, or apoptosis.[36]

Finally, going one step forward, this strategy was expanded by adding a specific biofunctionality to the IB-patterned substrates. As a proof of concept, we applied the developed methodology with one example of biologically active IBs formed by the human basic fibroblast growth factor (FGF). Figure 5 shows representative bright-field and merged fluorescence images of NIH/3T3 fibroblast cells cultured during 24 h on 5 and 20 μm striped patterns of FGF- and GFP-derived IBs printed with inks of 9 and 240 $\mu g \cdot mL^{-1}$ concentrations of the IBs, respectively. Remarkable is the fact that NIH/3T cells are guided by the biofunctional FGF-derived IBs with a similar extension than with the GFP-IBs in spite of using a much lower concentration of IBs. This result cannot only be due to surface topography and geometry of the pattern but also to the bioactivity of FGF-derived IBs since it has been recently shown that FGF-derived IBs retain the biologic activity of the protein,[37] and that the protein is released from IBs for a biological effect on the cells. This is due to a particular sponge-like architecture of these IBs[38] that permits a sustained delivery of the protein forming the IBs to the extracellular media or to target cell compartments.[39−41] Figures S15 and S16 show the positive influence of the FGF-derived IB patterns on cells orientation. In fact, the spindle-like distribution observed is an indication of the cell membrane alignment to the horizontal direction following the patterned stripes and thus a strong guidance of the orientation. This tendency is much stronger after the first 24 h of culture and weakens as cell density increases with time, consistent with our previous studies.

The control of cell positioning and spatial orientation is crucial in tissue engineering, especially for

attempting the generation of complex structures and axonal projections in nervous regeneration, blood vessel engineering, and construction of stable multilayered artificial tissues.[42,43] Although the external supply of soluble factors is widely used in this field, supported by the emerging understanding of signaling cascades, it tends toward acting in terms of proliferation and differentiation rather than intervening in cell orientation and positioning. Both biological and mechanical stimuli in combination with these factors seem to be the best approach to the mimicry of real cell environments.[34] On the other hand, magnetic force-based tissue engineering[44] permits the distal control of cell types in homogeneous and heterogeneous tissues[45] but not a true 2D guidance of cells, organelles, and projections. On the contrary, the use of patterned substrates permits control of the expression of cell adhesion molecules,[46] the distribution of focal adhesions,[47] and the orientation of whole cells, as well as the morphological appearance.[48,49] Grooved or pitted surfaces offer valuable models for top-down topographies, while the bottom-up surface decoration with carbon nanotubes, ceramics, and other nano- or microstructured hard materials is methodologically simpler in determining cell responses to their environment. Unfortunately, a further application of these approaches to *in vivo* situations is bottlenecked by methodological constraints and biocompatibility issues, respectively. Bacterial IBs, which upon microprinting as defined patterns intervene as powerful cell guidance tools, offer intriguing properties and structural and functional versatility superior to those exhibited by other materials used for decoration. The adjustable size, shape, adhesiveness, stiffness, ζ-potential, density, biocompatibility, and biodegradability of IBs,[24] apart from their cost-effective production and functionality of the protein forming de IBs,[39−41] make them unique soft materials and promising emerging tools for complex applications in tissue engineering beyond their straightforward utility as enhancers of substrate colonization and cell proliferation.

CONCLUSIONS

We have successfully engineered at the microscale supports by decorating them with a novel protein-based nanomaterial, based on bacterial IBs, using a modification of the μCP technique that allows increasing the mass transfer of IBs from the stamps to the substrates. After a first optimization of the IB density used for the patterning, we have cultured fibroblast cells over these supports and established a protocol to investigate IB-based regulation of cellular functions. One of the contributions of this study relies on the design of a methodology for the statistical analysis of images of cells cultured at different times over patterns of IBs, with various geometries and densities, to study the behavior of cells. This method of analysis represents a new useful and generic tool for other researchers in the field. Specifically, in the present work, these analyses enabled the study of the influence of different microscale structuring of IBs on the orientation, morphology, and positioning of cells, demonstrating the importance of 2D microscale engineering and the usefulness of the IB nanoscale profiling for cell guidance. We have shown that cells preferentially adhere to IB-rich areas, aligning and elongating according to the IB pattern and choosing the shortest way to reach new adhesion spots on the IBs. This 2D engineering technique based on IBs fills the gap between existing techniques which are based on the local modification of the chemical nature of the surface and those based on the modification of the topography at the nanoscale level by physical methods because IBs combine at the same time biofunctionalization and topographical modification of the roughness. It has therefore proved that IBs are interesting and useful nanomaterials in the control of cell culture as well as promising biomaterials for regenerative medicine.

MATERIALS AND METHODS

Phosphate Buffered Saline (PBS) Solution Preparation. Store solution of concentrated PBS was obtained by dissolving NaCl (5.494 g), Na_2HPO_4 (0.44 g), and NaH_2PO (0.108 g) in MilliQ water (1 l). Sodium hydroxide was used to obtain pH 7.4. Solution was diluted 10 times before use.

Bacterial Cells, Plasmids, and IB Production. IBs were produced in *E. coli* derivative strain JGT20 (dnak756 thr::Tn10).[50] This strain was transformed with the expression vector pTVP1GFP (ApR), encoding for a green fluorescent protein (GFP) fused at the amino terminus to VP1, a hydrophobic capsid protein from foot-and-mouth disease virus,[51] which promotes deposition as IBs.[52] IBs of FGF-2 (155 amino acid isoform, 18 kDa) were produced in *Escherichia coli* BL21(DE3), transformed with the vector pET29c-(+)-hFGF-2.[53] FGF-2 protein did not contain any additional pull-down protein to induce IB formation. The recombinant genes were expressed under the control of an IPTG inducible-trc promoter. Bacterial cells were cultured in shake flasks using LB-rich medium supplemented with the required antibiotics. When cultures reached an OD_{550} of 0.5 protein expression and therefore IB formation was induced by adding 1 mM IPTG at 37 °C (GFP) and 25 °C (FGF-2). Samples were taken 3 h postinduction.

IB Purification. Bacterial cell cultures were treated by adding lysozyme and PMSF at 1 mg/mL and 0.4 mM, respectively, and incubating them for 2 h at 37 °C. Lysozyme treatment attacked bacterial cell wall, facilitating subsequent cell disruption by mechanical procedures. Samples were frozen at −80 °C to release the IBs and washed in Triton X-100 1% (v/v) for 1 h at room temperature. After that, samples were frozen again at −80 °C. An additional washing step was carried out by adding Nonidet P-40 detergent 0.03% (v/v) and incubating IBs for 1 h at 4 °C. Mild detergent washings were used for removing cell membranes from the IB. Next, samples were treated with 1 μg/mL DNase in the presence of 1 mM $MgSO_4$ for 1 h at 37 °C in order to get rid of contaminant DNA. Finally, the absence of alive bacteria in the IB preparations was tested by plating 100 μL of sample on LB plates incubated overnight at 37 °C. Samples were frozen/thawed until no viable bacteria were observed. Finally, IB samples were centrifuged for 15 min at 15 000*g*, and pellets

were stored at −80 °C until further use. Purified IBs were quantified by Western blot using Quantity One software (Bio-Rad) to analyze band intensity and infer protein concentration from a GFP standard curve or BSA standard curve in the case of FGF-2 IBs.

Amino-Terminated SAM Deposition. Silicon wafers (100) (SiMat, Germany) covered with native SiO_2 were cut in small 1 cm^2 pieces. Substrates were placed in piranha solution [concentrated sulfuric acid, (Panreac, Spain)/33% aqueous hydrogen peroxide (Aldrich), 7:3] for 15 min, copiously rinsed with ultrapure water (Advantage A10 water purification system, Millipore) and HPLC grade ethanol (Tecnokroma, Spain), and dried under a stream of pure nitrogen. Then substrates were introduced into a desiccator with a flask with 0.1 mL of *N*-[3-(trimethoxysilyl)propyl]ethylenediamine (Aldrich). The system was left under vacuum overnight at 36 °C to obtain a complete amino-terminated SAM covering the SiO_2 surface.

Microcontact Printing. PDMS stamps were fabricated by casting a 10:1 (v/v) mixture of PDMS and curing agent (Sylgard 184, Dow Corning) against a photolithographically patterned silicon master, degassed in desiccator, cured for 18 h at 60 °C, and released. In order to overcome problems with IB transfer from the suspension to the substrates, we have used a modification of the μCP procedure. Thus, before soaking the stamp in the IB suspension, the stamps were sonicated for 5 min in acetone, exposed to vacuum for 10 min, sonicated in a sodium dodecyl sulfate (SDS) (Sigma) solution (10% w/w in MiliQ water) for 5 min, conditioned in the same media for 5 min, dried with a N_2 flow, dipped in MilliQ water to remove the excess of SDS, and dried again with a N_2 stream. After the pretreatment, stamps were inked with the suspension of IBs in PBS solution (pH 7.5) for 20 min, dried under a nitrogen flow, and placed on the clean amine-terminated silicon substrate under a 10 g weight. After 1 min of contact, the stamp was carefully removed. Suspensions of differently concentrated IBs were used for the study (489, 244, and 30 μg mL^{-1}). The concentration of GFP-derived IBs used for the study of cell guidance was 244 μg mL^{-1}, and with FGF-derived IBs, it was 9.0 μg mL^{-1}. Each stamp was used no more than four times and within 1 week from production. Random patterns were produced using the flat side of the stamp. When not in use, the stamps were always stored in MilliQ water.

Cell Culture and Cell Dyes for Microscopy Analysis. Prior to the cell seeding, substrates were shuffled and gently rinsed with DPBS, blocked with BSA (3% w/w in PBS), rinsed again with DPBS, and introduced into the 24-wells plate (Nunclon).

1BR3.G and NIH/3T3 cells were routinely cultured in DMEM (Dulbecco's modified Eagle medium) supplemented with 2 mM L-glutamine and 10% FBS (v/v) at 37 °C and 10% CO_2 in a humidified incubator. In the case of NIH/3T3 cells, 24 h prior to the seeding over supports, the medium was switched with a low serum DMEM containing 1% FBS (v/v). Cells were seeded at density 3×10^4 per well and incubated in (2 mL) DMEM supplemented with 2 mM L-glutamine, gentamicine (50 μg mL^{-1}), and 10% (1BR3.G) or 1% (NIH/3T3) of FBS.

After cultivation, supports were rinsed with DPBS, cells were fixed with 4% paraformaldehyde for 30 min with gentle agitation, and rinsed again with DPBS. Then DPBS with fluorescent dyes, red CellMask (Invitrogen) for membrane and blue Hoescht (Invitrogen) for nuclei (1 and 0.2 μL mL^{-1}, respectively), were added, and the plate was incubated for 10 min at room temperature with agitation. Once again, supports were rinsed with DPBS.

Optical and Confocal Microscopy. Supports were observed under an Olympus BX51 microscope equipped with an Olympus DP20 CCD camera. Fluorescence images were obtained with an Olympus U-LH100HG UV lamp and the adequate filters. Magnification of 50× was used to obtain images for the statistical treatment. Images were taken randomly from at least three different regions from different supports. The time of exposure was 1 s for the nuclei and a maximum of 8 s for cell membranes and GFP IBs. For the study of IB density on surfaces, specific care was taken to acquire images always under the same exposure conditions. In order to obtain confocal microscopy images, samples were mounted on 35 mm dishes (IBIDI, Germany) with Fluoprep (Bio-Merieux, France). A Leica TCS SP5 AOBS spectral confocal microscope (Leica Microsystems, Mannheim, Germany) with a Plan-Apochromat 63×, 1.4 NA lens was used. Membranes, nuclei, and IBs were excited with a 405 nm diode laser beam, 633 nm helium neon laser beam, and a 488 nm argon laser beam, respectively, and detected at 414−461, 656−789, and 500−537 nm, respectively.

Image Analysis. Cell localization, orientation, and morphology data were extracted from images using the ImageJ software and treated with MS Excel and Gnuplot. The minimum number of data points used to perform the statistical analysis was 120 in all cases.

Cell Positioning. Specific care was taken to ensure that the treatment was the same for all the images taken from the same area. First, images were numerically rotated to align stripes (or rows of dots) horizontally. Then, the "plot profile" command of ImageJ was performed over a rectangular selection to calculate the average intensity of luminescence per pixel line. The results describe the average luminescent occurrence of membrane (red), nuclei (blue), or IBs (green) *versus* the distance. The profile plots were normalized so that the minimum value is 0 and the maximum 1 and then subsequently juxtaposed. We approximated the actual profile of IBs' fluorescence with the "ideal" patterning assuming a value of 0 between stripes and 1 for stripes (or circular distribution for dotted pattern). These values were normalized taking into account the overall surface of patterned and unpatterned stripes within the inspected area. Dotted pattern was analyzed in two directions (horizontal and vertical). It is important to note that in the case of dotted patterns only 19% of the surface was printed with IBs.

Cell Orientation. The aligned images were turned into black and white with the threshold tools of the ImageJ software. Then geometrical parameters of each cell were automatically calculated with the ImageJ "Analyze particles" procedure. Each region corresponding to the investigated feature (cell membrane or nuclei) was approximated to an ellipse. The angle between the long-axis of the ellipse and the *x*-axis of the image (direction of stripe or dot lines) was calculated. Moreover, the area of each region was calculated, and only areas with surface greater than 100 μm^2 were considered for further analysis. Data from different images but corresponding to the same growth conditions were joined. The frequencies of angle orientation were separated into 10° wide bins from 0 to 180° and represented as radial plots. Values between 180 and 360° are symmetric repetition of data added for convenience. Additional analysis of the Gini coefficient is presented in the Supporting Information.

Cell Morphology. Each cell was approximated to an ellipse, and its elongation was calculated as a ratio between the longest and shortest axes minus one. Average values and standard errors were calculated in all cases.

Proliferation Analysis. The results of the colorimetric assays are described and summarized in the Supporting Information.

Conflict of Interest: The authors declare no competing financial interest.

Acknowledgment. The authors are indebted to the Cell Culture Unit of the "Servei de Cultius Cellulars, Producció d'Anticossos i Citometria" (SCAC), and to the "Servei de Microscòpia", both at the UAB. We are also indebted to the Protein Production Platform (CIBER-BBN) for helpful technical assistance (http://bbn.ciber-bbn.es/programas/plataformas/equipamiento). This work was supported by the DGI Grant POMAs (CTQ2010-19501), the MICIN Project BFU2010-17450, AGAUR (Grants SGR2009-516 and 2009SGR-108), the Networking Research Center on Bioengineering, Biomaterials, and Nanomedicine (CIBER-BBN). E.G.F. is supported by the Programa Personal de Técnico de Apoyo (Modalidad Infraestructuras científico-tecnológicas, MICINN). W.I.T. is grateful to the Consejo Superior de Investigaciones Científicas (CSIC) for a "JAE-pre" fellowship, and K.P. to the Erasmus scholarship. J.S.-F. is the recipient of a PIF doctoral fellowship from UAB and AV of an ICREA ACADEMIA award.

Supporting Information Available: Representative images as well as detailed comparison of cell orientation (membrane and nuclei), morphology, and position, as well as further discussion about the validity of the used method and the pattern quality. This material is available free of charge *via* the Internet at http://pubs.acs.org.

REFERENCES AND NOTES

1. Philipsborn, A. C.; Lang, S.; Bernard, A.; Loeschinger, J.; David, C.; Lehnert, D.; Bastmeyer, M.; Bonhoeffer, F. Microcontact Printing of Axon Guidance Molecules for Generation of Graded Patterns. *Nat. Protoc.* **2006**, *1*, 1322–1328.
2. Falconnet, D.; Csucs, G.; Grandin, H. M.; Textor, M. Surface Engineering Approaches To Micropattern Surfaces for Cell-Based Assays. *Biomaterials* **2006**, *27*, 3044–3063.
3. Ruiz, S. A.; Chen, C. S. Microcontact Printing: A Tool To Pattern. *Soft Matter* **2007**, *3*, 168–177.
4. Mrksich, M.; Dike, L. E.; Tien, J.; Ingber, D. E.; Whitesides, G. M. Using Microcontact Printing To Pattern the Attachment of Mammalian Cells to Self-Assembled Monolayers of Alkanethiolates on Transparent Films of Gold and Silver. *Exp. Cell. Res.* **1997**, 305–313.
5. Zhang, S.; Yan, L.; Altman, M.; Lässle, M.; Nugent, H.; Frankel, F.; Lauenburger, D. A.; Whitesides, G. M.; Rich, A. Biological Surface Engineering: A Simple System for Cell Pattern Formation. *Biomaterials* **1999**, *20*, 1213–1220.
6. Zhang, J.; Nie, J.; Mühlstädt, M.; Gallagher, H.; Pullig, O.; Jandt, K. D. Stable Extracellular Matrix Protein Patterns Guide the Orientation of Osteoblast-like Cells. *Adv. Funct. Mater.* **2011**, *20*, 1–9.
7. Lange, S. A.; Benes, V.; Kern, D. P.; Horber, J. K. H.; Bernard, A. Microcontact Printing of DNA Molecules. *Anal. Chem.* **2004**, *76*, 1641–1653.
8. Yoo, S. Y.; Chung, W. J.; Kim, T. H.; Le, M.; Lee, S. W. Facile Patterning of Genetically Engineered M13 Bacteriophage for Directional Growth of Human Fibroblast Cells. *Soft Matter* **2011**, *7*, 363–368.
9. Raghavan, S.; Desai, R. A.; Kwon, Y.; Mrksich, M.; Chen, C. S. Micropatterned Dynamically Adhesive Substrates for Cell Migration. *Langmuir* **2010**, *26*, 17733–17738.
10. Yan, X.; Yao, J.; Lu, G.; Chen, X.; Zhang, K.; Yang, B. Microcontact Printing of Colloidal Crystals. *J. Am. Chem. Soc.* **2004**, *126*, 10510–10511.
11. Weibel, D. B.; Lee, A.; Mayer, M.; Brady, S. F.; Bruzewicz, D.; Yang, J.; DiLuzio, W. R.; Clardy, J.; Whitesides, G. M. Bacterial Printing Press That Regenerates Its Ink: Contact-Printing Bacteria Using Hydrogel Stamps. *Langmuir* **2005**, *21*, 6436–6442.
12. Martinez, E.; Engel, E.; Planell, J. A.; Samitier, J. Effects of Artificial Micro- and Nano-Structured Surfaces on Cell Behaviour. *Ann. Anat.* **2009**, *191*, 126–135.
13. Bettinger, C. J.; Langer, R.; Borenstein, J. T. Engineering Substrate Topography at the Micro- and Nanoscale To Control Cell Function. *Angew. Chem., Int. Ed.* **2009**, *48*, 5406–5415.
14. Clark, P.; Connolly, P.; Curtis, A. S. G.; Dow, J. A. T.; Wilkinson, C. D. W. Cell Guidance by Ultrafine Topography *in Vitro*. *J. Cell Sci.* **1991**, *99*, 73–77.
15. Dalby, M. J.; Gadegaard, N.; Riehle, M. O.; Wilkinson, C. D. W.; Curtis, A. S. G. Investigating Filopodia Sensing Using Arrays of Defined Nano-Pits down to 35 nm Diameter in Size. *Int. J. Biochem. Cell Biol.* **2004**, *36*, 2005–2015.
16. Teixeira, A. I.; Abrams, G. A.; Bertics, P. J.; Murphy, C. J.; Nealey, P. F. Epithelial Contact Guidance on Well-Defined Micro- and Nanostructured Substrates. *J. Cell Sci.* **2003**, *116*, 1881–1892.
17. Abdullah, C. A. C.; Asanithi, P.; Brunner, E. W.; Jurewicz, I.; Bo, C.; Azad, C. L.; Ovalle-Robles, R.; Fang, S.; Lima, M. D.; Lepro, X.; *et al.* Aligned, Isotropic and Patterned Carbon Nanotube Substrates That Control the Growth and Alignment of Chinese Hamster Ovary Cells. *Nanotechnology* **2011**, *22*, 205102.
18. Kang, K.; Choi, S. E.; Jang, H. S.; Cho, W. K.; Nam, Y.; Choi, I. S.; Lee, J. S. *In-Vitro* Developmental Acceleration of Hippocampal Neurons on Nanostructures of Self-Assembled Silica Beads in Filopodium-Size Ranges. *Angew. Chem., Int. Ed.* **2011**, *50*, 1–5.
19. Charest, J. L.; Eliason, M. T.; Garcia, A. J.; King, W. P. Combined Microscale Mechanical Topography and Chemical Patterns on Polymer Cell Culture Substrates. *Biomaterials* **2006**, *27*, 2487–2494.
20. Feinberg, A. W.; Wilkerson, W. R.; Seegert, C. A.; Gibson, A. L.; Hoipkemeier-Wilson, L.; Brennan, A. B. Systematic Variation of Microtopography, Surface Chemistry and Elastic Modulus and the State Dependent Effect on Endothelial Cell Alignment. *J. Biomed. Mater. Res., Part A* **2008**, *86*, 522–534.
21. Recknor, J. B.; Sakaguchi, D. S.; Mallapragada, S. K. Directed Growth and Selective Differentiation of Neural Progenitor Cells on Micropatterned Polymer Substrates. *Biomaterials* **2006**, *27*, 4098–4108.
22. Rivera-Gil, P.; Yang, F.; Thomas, H.; Li, L.; Terfort, A.; Parak, W. J. Development of an Assay Based on Cell Counting with Quantum Dot Labels for Comparing Cell Adhesion within Cocultures. *Nano Today* **2011**, *6*, 20–27.
23. Rodríguez-Carmona, E.; Villaverde, A. Nanostructured Bacterial Materials for Innovative Medicines. *Trends Microbiol.* **2010**, *18*, 423–430.
24. García-Fruitós, E.; Vazquez, E.; Díez-Gil, C.; Corchero, J. L.; Seras-Franzoso, J.; Ratera, I.; Veciana, J.; Villaverde, A. Bacterial Inclusion Bodies: Making Gold from Waste. *Trends Biotechnol.* **2012**, *30*, 65–70.
25. García-Fruitós, E.; Seras-Franzoso, J.; Vazquez, E.; Villaverde, A. Tunable Geometry of Bacterial Inclusion Bodies as Substrate Materials for Tissue Engineering. *Nanotechnology* **2010**, *21*, 205101.
26. Rodríguez-Carmona, E.; Cano-Garrido, O.; Seras-Franzoso, J.; Villaverde, A.; García-Fruitós, E. Isolation of Cell-Free Bacterial Inclusion Bodies. *Microb. Cell Fact.* **2010**, *9*, 71.
27. García-Fruitós, E.; Rodriguez-Carmona, E.; Díez-Gil, C.; Ferraz, R. M.; Vazquez, E.; Corchero, J. L.; Cano-Sarabia, M.; Ratera, I.; Ventosa, N.; Veciana, J.; *et al.* Surface Cell Growth Engineering Assisted by a Novel Bacterial Nanomaterial. *Adv. Mater.* **2009**, *21*, 4249–4253.
28. Díez-Gil, C.; Krabbenborg, S.; García-Fruitós, E.; Vazquez, E.; Rodríguez-Carmona, E.; Ratera, I.; Ventosa, N.; Seras-Franzoso, J.; Cano-Garrido, O.; Ferrer-Miralles, N.; *et al.* The Nanoscale Properties of Bacterial Inclusion Bodies and Their Effect on Mammalian Cell Proliferation. *Biomaterials* **2010**, *31*, 5805–5812.
29. Seras-Franzoso, J.; Díez-Gil, C.; Vazquez, E.; García-Fruitós, E.; Cubarsi, R.; Ratera, I.; Veciana, J.; Villaverde, A. Bioadhesiveness and Efficient Mechanotransduction Stimuli Synergistically Provided by Bacterial Inclusion Bodies as Scaffolds for Tissue Engineering. *Nanomedicine* **2012**, *7*, 79–93.
30. Mahmoudi, M.; Lynch, I.; Ejtehadi, M. R.; Monopoli, M. P.; Baldelli Bombelli, F.; Laurent, S. ProteinNanoparticle Interactions: Opportunities and Challenges. *Chem. Rev.* **2011**, *111*, 5610–5637.
31. Chang, J. C.; Brewer, G. J.; Wheeler, B. C.A. Modified Microstamping Technique Enhances Polylysine Transfer and Neuronal Cell Patterning. *Biomaterials* **2003**, *24*, 2863–2870.
32. Wood, M. A.; Wilkinson, C. D.; Curtis, A. S. The Effects of Colloidal Nanotopography on Initial Fibroblast Adhesion and Morphology. *IEEE Trans. Nanobiosci.* **2006**, *5*, 20–31.
33. Ballo, A.; Agheli, H.; Lausmaa, J.; Thomsen, P.; Petronis, S. Nanostructured Model Implants for *In Vivo* Studies: Influence of Well-Defined Nanotopography on *De Novo* Bone Formation on Titanium Implants. *Int. J. Nanomed.* **2011**, *6*, 3415–3428.
34. Dalby, M. J.; McCloy, D.; Robertson, M.; Agheli, H.; Sutherland, D.; Affrossman, S.; Oreffo, R. O. C. Osteoprogenitor Response to Semi-ordered and Random Nanotopographies. *Biomaterials* **2006**, *27*, 2980–2987.
35. Charest, J. L.; Garcia, A. J.; King, W. P. Myoblast Alignment and Differentiation on Cell Culture Substrates with Microscale Topography and Model Chemistries. *Biomaterials* **2007**, *28*, 2202–2210.
36. McNamara, L. E.; McMurray, R. J.; Biggs, M. J. P.; Kantawong, F.; Oreffo, R. O. C.; Dalby, M. J. Nanotopographical Control of Stem Cell Differentiation. *J. Tissue Eng.* **2010**, *2010*, 120623.
37. Seras-Franzoso, J.; Peebo, K.; Corchero, J. L.; Tsimbouri, M. P.; Unzueta, U.; Rinas, U.; Dalby, M. J.; Vazquez, E.; García-Fruitós, E.; Villaverde, A. A Nanostructured Bacterial Bio-Scaffold for the Sustained Bottom-up Delivery of Protein Drugs. *Nanomedicine* **2013**, 10.2217/NNM.12.188.

38. Cano-Garrido, O.; Rodríguez-Carmona, E.; Díez-Gil, C.; Vázquez, E.; Elizondo, E.; Cubarsi, R.; Seras-Franzoso, J.; Corchero, J. L.; Rinas, U.; Ratera, I.; *et al.* Supramolecular Organization of Protein-Releasing Functional Amyloids Solved in Bacterial Inclusion Bodies. *Acta Biomater.* **2013**, *9*, 6134–6142.
39. Villaverde, A. Bacterial Inclusion Bodies: An Emerging Platform for Drug Delivery and Cell Therapy. *Nanomedicine* **2012**, *7*, 1277–1279.
40. Villaverde, A.; García-Fruitós, E.; Rinas, U.; Seras-Franzoso, J.; Kosoy, A.; Corchero, J. L.; Vazquez, E. Packaging Protein Drugs as Bacterial Inclusion Bodies for Therapeutic Applications. *Microb. Cell Fact.* **2012**, *11*, 76.
41. Vazquez, E.; Corchero, J. L.; Burgueño, J. F.; Seras-Franzoso, J.; Kosoy, A.; Bosser, R.; Mendoza, R.; Martínez-Láinez, J. M.; Rinas, U.; Fernandez, E.; *et al.* Functional Inclusion Bodies Produced in Bacteria as Naturally Occurring Nanopills for Advanced Cell Therapies. *Adv. Mater.* **2012**, *24*, 1742–1747.
42. Hoffman-Kim, D.; Mitchel, J. A.; Bellamkonda, R. V. Topography, Cell Response, and Nerve Regeneration. *Annu. Rev. Biomed. Eng.* **2010**, *12*, 203–231.
43. Ito, A.; Hayashida, M.; Honda, H.; Hata, K.; Kagami, H.; Ueda, M.; Kobayashi, T. Construction and Harvest of Multilayered Keratinocyte Sheets Using Magnetite Nanoparticles and Magnetic Force. *Tissue Eng.* **2004**, *10*, 873–880.
44. Akiyama, H.; Ito, A.; Kawabe, Y.; Kamihira, M. Fabrication of Complex Three-Dimensional Tissue Architectures Using a Magnetic Force-Based Cell Patterning Technique. *Biomed. Microdevices* **2009**, *11*, 713–721.
45. Corchero, J. L.; Villaverde, A. Biomedical Applications of Distally Controlled Magnetic Nanoparticles. *Trends Biotechnol.* **2009**, *27*, 468–476.
46. Heydarkhan-Hagvall, S.; Choi, C.-H.; Dunn, J.; Heydarkhan, S.; Schenke-Layland, K.; MacLellan, W. R.; Beygui, R. Influence of Systematically Varied Nano-scale Topography on Cell Morphology and Adhesion. *Cell Commun. Adhes.* **2007**, *14*, 181–194.
47. Uttayarat, P.; Toworfe, G. K.; Dietrich, F.; Lelkes, P. I.; Composto, R. J. Topographic Guidance of Endothelial Cells on Silicone Surfaces with Micro- to Nanogrooves: Orientation of Actin Filaments and Focal Adhesions. *J. Biomed. Mater. Res.* **2005**, *75A*, 668–680.
48. McKee, C. T.; Raghunathan, V. K; Nealey, P. F; Russell, P.; Murphy, C. J. Topographic Modulation of the Orientation and Shape of Cell Nuclei and Their Influence on the Measured Elastic Modulus of Epithelial Cells. *Biophys. J.* **2011**, *101*, 2139–2146.
49. Peterbauer, T.; Yakunin, S.; Siegel, J.; Hering, S.; Fahrner, M.; Romanin, C.; Heitz, J. Dynamics of Spreading and Alignment of Cells Cultured *in Vitro* on a Grooved Polymer Surface. *J. Nanomater.* **2011**, 413079–413088.
50. Thomas, J. G.; Baneyx, F. Roles of the *Escherichia coli* Small Heat Shock Proteins IBPA and IBPB in the rmal Stress Management: Comparison with Clpa, Clpb, and HtpG *in Vivo*. *J. Bacteriol.* **1998**, *180*, 5165–5172.
51. García-Fruitós, E.; Gonzalez-Montalban, N.; Morell, M.; Vera, A.; Ferraz, R. M.; Aris, A.; Ventura, S.; Villaverde, A. Aggregation as Bacterial Inclusion Bodies Does Not Imply Inactivation of Enzymes and Fluorescent Proteins. *Microb. Cell Fact.* **2005**, *4*, 27.
52. Carrio, M.; Gonzalez-Montalban, N.; Vera, A.; Villaverde, A.; Ventura, S. Amyloid-like Properties of Bacterial Inclusion Bodies. *J. Mol. Biol.* **2005**, *347*, 1025–1037.
53. Hoffmann, F.; van den Heuvel, J.; Zidek, N.; Rinas, U. Minimizing Inclusion Body Formation during Recombinant Protein Production in *Escherichia coli* at Bench and Pilot Plant Scale. Enzyme. *Microb. Technol.* **2004**, *34*, 235–241.